

Activation cross-sections of longer-lived products of proton induced nuclear reactions on dysprosium up to 36 MeV

F. Tárkányi^a, F. Ditrói^{a,*}, S. Takács^a, A. Hermanne^b, A.V. Ignatyuk^c

^a*Institute for Nuclear Research of the Hungarian Academy of Sciences (ATOMKI), Debrecen, Hungary*

^b*Cyclotron Laboratory, Vrije Universiteit Brussel (VUB), Brussels, Belgium*

^c*Institute of Physics and Power Engineering (IPPE), Obninsk, Russia*

Abstract

Activation cross-sections of longer-lived products of proton induced nuclear reactions on dysprosium were measured up to 36 MeV by using stacked foil irradiation technique and γ -spectrometry. We report for the first time experimental cross-sections for the formation of the radionuclides ^{162m}Ho , ^{161}Ho , ^{159}Ho , ^{159}Dy , ^{157}Dy , ^{155}Dy , ^{161}Tb , ^{160}Tb , ^{156}Tb and ^{155}Tb . The experimental data were compared with the results of cross-section calculations of the ALICE and EMPIRE nuclear model codes and of the TALYS nuclear reaction model code as listed in the on-line libraries TENDL-2011 and TENDL-2012.

Keywords: dysprosium target, holmium, dysprosium and terbium radioisotopes, physical yield

1. Introduction

A research program is running to study activation cross-sections of proton and deuteron induced reactions mainly for practical applications and to test the presently used theoretical nuclear reaction codes. From a detailed study of the literature it was recognized that data on rare earth elements in most cases are missing. It is well known that many rare earth radionuclides are used in medicine for diagnostic (PET) and, in a larger proportion, for therapeutic (radiopharmaceuticals and brachytherapy) purposes. In the frame of this systematic study we have investigated the activation cross-sections induced by protons and deuterons on natural dysprosium targets. The part of the study specifically devoted to production of ^{161}Ho , a candidate therapeutic radioisotope, was published separately (Tárkányi et al., 2013a). Here we report on the complete set of activation cross-section data induced by proton irradiation of dysprosium. No earlier experimental data were found in the literature.

2. Experiment and data evaluation

The general characteristics and procedures for irradiation, activity assessment and data evaluation (including estimation of uncertainties) were similar as in many of our earlier works (Takács et al., 2011; Tárkányi et al., 2012). The main experimental parameters and the methods of data evaluation for the present study are summarized in Table 1 (Andersen and Ziegler, 1977; Bonardi, 1987; Canberra, 2000; Dityuk et al., 1998; Herman et al., 2007; International-Bureau-of-Weights-and-Measures, 1993; Kinsey et al., 1997; Koning and Rochman, 2012; Pritychenko and Sonzogni, 2003; Székely, 1985; Tárkányi et al., 1991, 2001). The used decay data are collected in Table 2. For beam current and beam energy monitoring and for energy degradation Ti foils were incorporated downstream of each dysprosium foils in the stack. All monitor foil data were considered simultaneously in order to obtain the beam current and beam energy in each target foil by comparison with the IAEA recommended monitor data (Tárkányi et al., 2001). The measured cross-sections of the monitor reaction and

*Corresponding author: ditroi@atomki.hu

the recommended data are shown in Fig. 1.

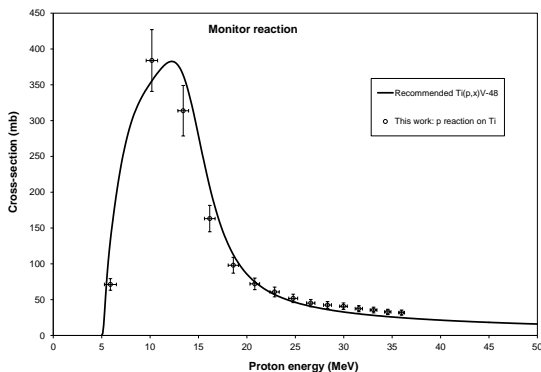


Figure 1: The simultaneously measured monitor reactions for determination of proton beam energy and intensity

3. Results and discussion

3.1. Cross-sections

The measured cross-sections for the production of ^{162m}Ho , ^{161}Ho , ^{159}Ho , ^{159}Dy , ^{157}Dy , ^{155}Dy , ^{161}Tb , ^{160}Tb , ^{156}Tb , ^{155}Tb are shown in Table 3-4 and Figures 2-11. The figures also show the theoretical results calculated with the ALICE-IPPE and the EMPIRE codes and the values available in the on-line libraries TENDL-2011 and TENDL-2012 in comparison with experimental results of this work. We show both TENDL versions, obtained from the standard set - not adjusted parameters - to illustrate the difference and the effect of the upgrading. Due to the experimental circumstances (stacked foil technique, large dose at EOB, limited detector capacity) no cross-section data were obtained for short-lived activation products as ^{164m}Ho (37.5 min), ^{164g}Ho (29 min), ^{162g}Ho (15.0 min), ^{160g}Ho (25.6 min), ^{158m}Ho (28 min), ^{157}Ho (12.6 min), ^{156}Ho (9.5 s, 7.8 min, 56 min) and ^{155}Ho , (48 min). Also the possibly produced radioisotopes ^{158}Tb (very long half-life, 180 a) and ^{160m}Ho (5.02 h) could not be identified in the measured spectra because of low energy unresolved γ -rays, or small effec-

tive cross-section due to the low abundance. The reactions are discussed separately for each reaction product. Naturally occurring dysprosium is composed of 7 stable isotopes (^{156}Dy - 0.06%, ^{158}Dy - 0.10%, ^{160}Dy - 2.34%, ^{161}Dy - 18.9%, ^{162}Dy - 25.5%, ^{163}Dy - 24.9% and ^{164}Dy - 28.2%). The relevant contributing reactions are collected in Table. 2. The holmium reaction products are produced only through (p,xn) reactions, the dysprosium products directly via (p,pxn) reactions and through the decay of holmium radio-parents, the terbium radioisotopes are produced through directly (p,2pxn) reactions (including complex particle emissions) and decay of simultaneously produced dysprosium radio-products.

3.1.1. $^{nat}\text{Dy}(p,xn)^{162m}\text{Ho}$ reaction

Cross-sections for the short-lived ^{162g}Ho ground state ($T_{1/2} = 15.0$ min) were not measured. Theoretical estimates of ^{162m}Ho ($T_{1/2} = 67.0$ min) in TENDL 2011 and 2012 are systematically higher by a factor of 1.3 than our experimental results (Fig. 2). In case of ALICE-D and EMPIRE-D the agreement with the experiment is much better. To demonstrate the overestimation of TENDL, $0.7 \cdot \text{TENDL-2012}$ results were also presented, which gives a good estimation in shape and value of the new experimental data.

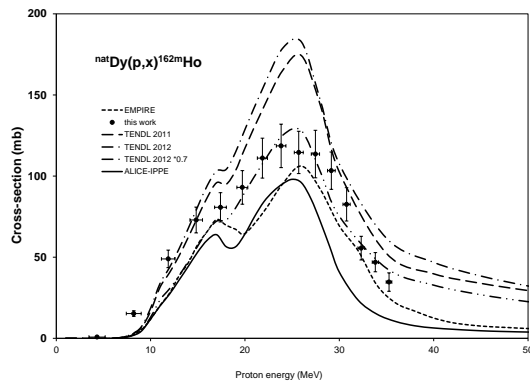


Figure 2: Experimental and theoretical cross-sections for the formation of ^{162m}Ho by the proton bombardment of dysprosium

Table 1: Main parameters of the experiment and the methods of data evaluations

Experiment		Data evaluation	
Incident particle	Proton	γ -spectra evaluation	Genie 2000, FORGAMMA (Canberra, 2000; Székely, 1985)
Method	Stacked foil	Determination of beam intensity	Faraday cup (preliminary) Fitted monitor reaction (final) (Tárkányi et al., 1991)
Target stack and thicknesses	Ti-Al-Dy-Al block Repeated 15 times <i>nat</i> Ti foil, 10.9 mm <i>nat</i> Al foil, 98 mm <i>nat</i> Dy foil, 100.59 mm	Decay data	NUDAT 2.6 (?)
Number of Dy target foils	15	Reaction Q-values	Q-value calculator (Pritychenko and Sonzogni, 2003)
Accelerator	CGR 560 cyclotron Vrije Universiteit Brussels	Determination of beam energy	(Andersen and Ziegler, 1977) (preliminary) Fitted monitor reaction (final) (Andersen and Ziegler, 1977)
Primary energy	36 MeV	Uncertainty of energy	Cumulative effects of possible uncertainties
Irradiation time	71 min	Cross-sections	Isotopic cross-section
Beam current	61 nA	Uncertainty of cross-sections	Sum in quadrature of all individual contribution (International-Bureau-of-Weights-and-Measures, 1993)
Monitor reaction [recommended values]	<i>nat</i> Ti(p,x) ⁴⁸ V reaction (Tárkányi et al., 2001)	Yield	Physical yield (Bonardi, 1987)
Monitor target and thickness	<i>nat</i> Ti, 10.9 mm	Theory	ALICE-IPPE (Dityuk et al., 1998) EMPIRE (Herman et al., 2007) TALYS (TENDL 2011, 2012 (Konig and Rochman, 2012))
detector	HPGe		
γ -spectra measurements	4 series		
Cooling times	1.5 h, 20 h, 80 h, 330 day		

3.1.2. *nat*Dy(p,xn)¹⁶¹Ho reaction

The experimental and theoretical cross-sections of the reactions producing ¹⁶¹Ho ($T_{1/2} = 2.48$ h) are shown in Fig. 3. The theoretical overestimation in all cases is significant. Scaling by a factor 0.7 of the TENDL-2011 results shows a rather good agreement.

3.1.3. *nat*Dy(p,xn)¹⁵⁹Ho reaction

The theory follows both in shape and in magnitude the experimental cross-sections of the ¹⁵⁹Ho ($T_{1/2} = 33.05$ min) in the investigated energy range (Fig. 4), as far as the TENDL calculations regarded. The ALICE-IPPE and EMPIRE overestimate again.

3.1.4. *P^{nat}*Dy(p,x)¹⁵⁹Dy reaction

The cumulative cross-sections of reactions producing ¹⁵⁹Dy ($T_{1/2} = 144.4$ d) contain apart from the direct production, the contribution from the decay of ¹⁵⁹Ho ($T_{1/2} = 33.05$ min) as they were measured after nearly complete decay of the parent isotope. The agreement with the results of the 3 codes is acceptable (Fig. 5). The TENDL results show that the direct production is negligible, especially below 30 MeV.

3.1.5. *nat*Dy(p,x)¹⁵⁷Dy reaction

The cumulative cross-sections for production of ¹⁵⁷Dy ($T_{1/2} = 8.14$ h) were measured after nearly complete decay of the parent ¹⁵⁷Ho ($T_{1/2} = 12.6$ min). The theoretical data overestimate the experimental results and here also the TENDL results show that the direct production is negligible (Fig. 6).

3.1.6. *nat*Dy(p,x)¹⁵⁵Dy reaction

The measured ¹⁵⁵Dy ($T_{1/2} = 9.9$ h) was produced directly and through decay of the ¹⁵⁵Ho ($T_{1/2} = 48$ min) parent radioisotope. The comparison with the TENDL results shows good agreement below 30 MeV (Fig. 7), and the agreement with the ALICE-IPPE and the EMPIRE results is also good below 25 MeV.

3.1.7. *nat*Dy(p,x)¹⁶¹Tb reaction

The measured direct cross-sections for production of ¹⁶¹Tb ($T_{1/2} = 6.89$ d) are shown in Fig. 8. As can be seen in Table 2 and 3, reactions on stable Dy target isotopes with nearly the same abundance can contribute to the production of ¹⁶¹Tb. From systematics it is known that the (p,2p) reaction has mostly lower cross-sections

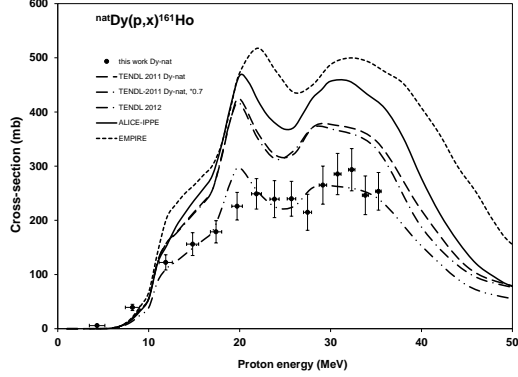


Figure 3: Experimental and theoretical cross-sections for the formation of ^{161}Ho by the proton bombardment of dysprosium

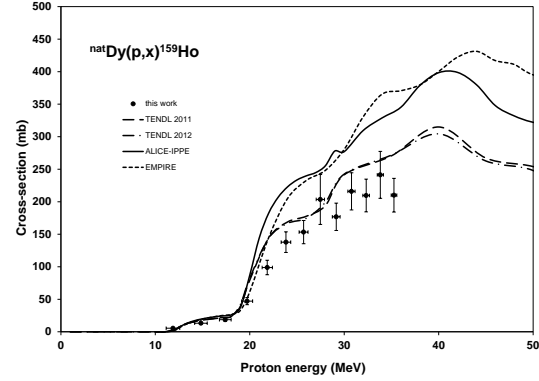


Figure 4: Experimental and theoretical cross-sections for the formation of ^{159}Ho by the proton bombardment of dysprosium

than the (p,2pn) channel. The sharp low energy peak due to $^{164}\text{Dy}(p, p)$ that can be seen in the TENDL theoretical data is hence questionable and is not reproduced by the experimental values, neither by the EMPIRE nor by ALICE results. It has to be mentioned too that the three codes provide very different results both in shape and in magnitude.

3.1.8. $n^{nat}\text{Dy}(p,xn)^{160}\text{Tb}$ reaction

Here also a sharp peak is predicted by the TENDL (Fig. 9) around 20 MeV, but according to physics expectation, the results of other model codes and to the experiment, no such peak is present in the excitation function of the ^{160}Tb ($T_{1/2} = 72.3$ d) in the investigated energy range. EMPIRE and ALICE describe well the shape but overestimate, respectively underestimate by a factor of two the experimental values.

3.1.9. $^{nat}\text{Dy}(p,xn)^{156}\text{Tb}$ reaction

The cross-sections of ^{156g}Tb ($T_{1/2} = 5.35$ d) were obtained from spectra measured after complete decay of the 2 isomeric states ($T_{1/2} = 5.3$ h, IT: 100 % and $T_{1/2} = 24.4$ h, IT: 100 %). In the investigated energy range there is a good resemblance between the data from ALICE the experimental data (Fig. 10). In this case TENDL-2011 and TENDL-2012 do not present a peaked structure but

underestimate the experimental cross-sections while EMPIRE again overestimates by a factor of 3.

3.1.10. $^{nat}\text{Dy}(p,xn)^{155}\text{Tb}$ reaction

The measured cross-sections of ^{155}Tb ($T_{1/2} = 5.32$ d) contains the complete contribution from the decay of ^{155}Dy ($T_{1/2} = 9.9$ h). The theories predict cross-sections close to the experimental data in the investigated energy range (Fig. 11).

3.2. Integral yields

The integral yields calculated from spline fits to our experimental excitation functions are shown in Fig 12 and Fig. 13. The integral yields represent so called physical yields i.e. activity instantaneous production rates at 1 μA beam current (Bonardi, 1987). The only literature value found is for ^{161}Ho (Stephens, 2010), which is about 30% lower than our calculated curve. From Fig. 12. It is seen that the produced radio-isotopes form two groups from the point of view of production yield. The production of holmium radio-isotopes begins at much lower bombarding energies and the production yields are also 3-4 orders of magnitude higher, that's why this figure was plotted with logarithmic scale. In Fig. 13 the terbium radio-isotopes are presented. The most promising is the

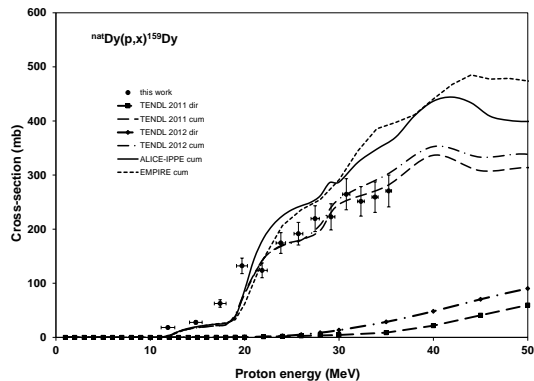


Figure 5: Experimental and theoretical cross-sections for the formation of ^{159}Dy by the proton bombardment of dysprosium

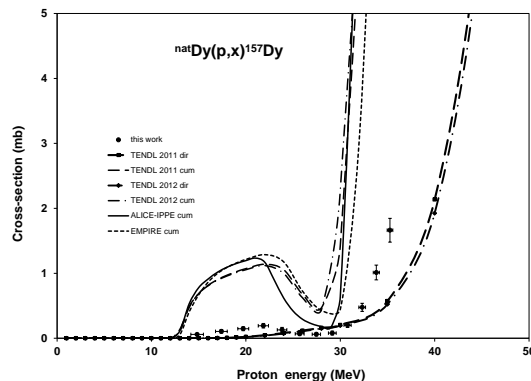


Figure 6: Experimental and theoretical cross-sections for the formation of ^{157}Dy by the proton bombardment of dysprosium

^{161}Tb both from the point of view of production yield and threshold of the production.

4. Summary and applications

We present the first experimental cross-sections for the $^{nat}\text{Dy}(p,x)$ ^{162m}Ho , ^{161}Ho , ^{159}Ho , ^{159}Dy , ^{157}Dy , ^{155}Dy , ^{161}Tb , ^{160}Tb , ^{156}Tb and ^{155}Tb nuclear reactions up to 36 MeV incident proton energy. Our excitation functions are relative to the $^{nat}\text{Ti}(p,n)^{48}\text{V}$ monitor reaction measured simultaneously. The experimental data were compared with the results obtained by the TALYS code reported in the TENDL libraries and with the results of ALICE-IPPE and EMPIRE calculations. The theoretical description, even for these proton induced reactions, is disappointing and gives disagreements. While for the (p,xn) reactions, resulting in Ho radionuclides, the predicted shapes are rather well corresponding to the contributions on multiple stable target nuclides, the absolute values are sometimes too high, sometimes too low by 50 to 100% and without a systematic behavior of each code. For formation of Dy, reactions with emission of a proton and decay of parent radionuclides are involved, the agreement between the different codes and the experimental values is better. The discrepancies are probably due to poor description of the parent Ho radionuclides cross-sections as the direct

reaction cross-sections are representing less than 10 % of the cumulative production. For Tb radionuclides in some cases the calculated excitation functions are well representing the experimental results but again disagreements in amplitude and non-physical peaks are appearing with no systematic behavior for "good" or "bad" codes. The differences between the two versions of the TENDL libraries are minimal and appear mostly as differences in amplitude of the order of 10% and especially at energies above 30 MeV. The experimental data continue hence to be important for testing the predictivity and improving the performances of the model codes, taking into account that no other experimental activation data are available for these reactions. The experimental results are of importance for several practical applications. Among the investigated reaction products we can mention:

- the radio-lanthanide ^{161}Ho ($T_{1/2} = 6.9$ d) is a promising Auger-electron emitter for internal radiotherapy, (Neves et al., 2005; Rosch, 2007; Stephens, 2010; Stephens and Mendenhall, 2010; Uusijarvi et al., 2006)
- The radionuclide ^{159}Dy ($T_{1/2} = 144$ d, EC = 100%) is a pure Auger electron and X-ray emitter and has gained interest in transmission imaging and bone mineral analysis (Nayak and Lahiri, 1999),

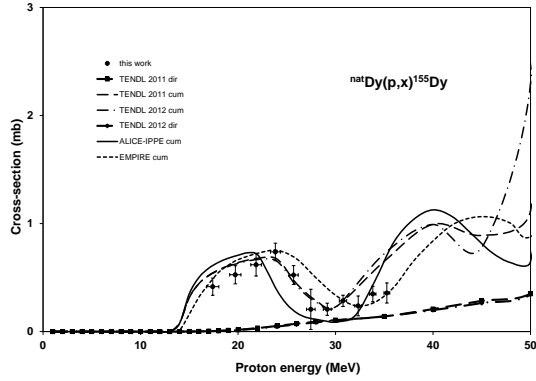


Figure 7: Experimental and theoretical cross-sections for the formation of ^{155}Dy by the proton bombardment of dysprosium

while ^{157}Dy ($T_{1/2} = 8.14$ h.) (Lebowitz and Greene, 1971), was investigated as a bone seekers in the evaluation of bone lesions (Hubner et al., 1977).

Terbium offers 4 clinically interesting radioisotopes with complementary physical decay characteristics: ^{149}Tb , ^{152}Tb , ^{155}Tb , and ^{161}Tb . The identical chemical characteristics of these radioisotopes allow the preparation of radiopharmaceuticals with identical pharmacokinetics useful for PET (^{152}Tb) or SPECT diagnosis (^{155}Tb) and for α - (^{149}Tb) and β^- -particle (^{161}Tb) therapy (Muller et al., 2012). From Dy targets the higher mass ^{155}Tb (decay of ^{155}Dy) and ^{161}Tb can be obtained, but we showed in a recent publication that other production methods are better (Tárkányi et al., 2013b). Production routes on other elemental targets have to be considered for $^{149,152}\text{Tb}$.

5. Acknowledgements

This work was performed in the frame of the HAS-FWO Vlaanderen (Hungary-Belgium) project. The authors acknowledge the support of the research project and of the respective institutions.

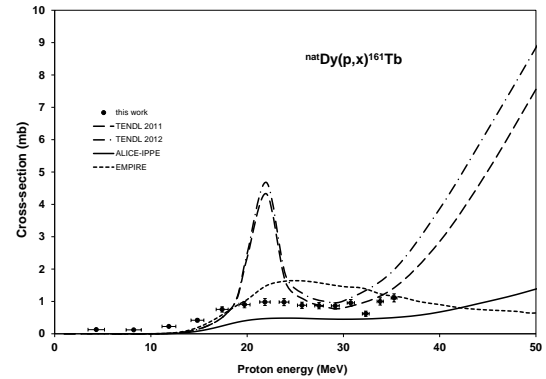


Figure 8: Experimental and theoretical cross-sections for the formation of ^{161}Tb by the proton bombardment of dysprosium

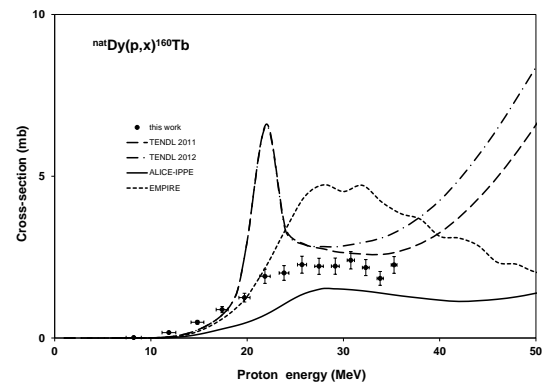


Figure 9: Experimental and theoretical cross-sections for the formation of ^{160}Tb by the proton bombardment of dysprosium

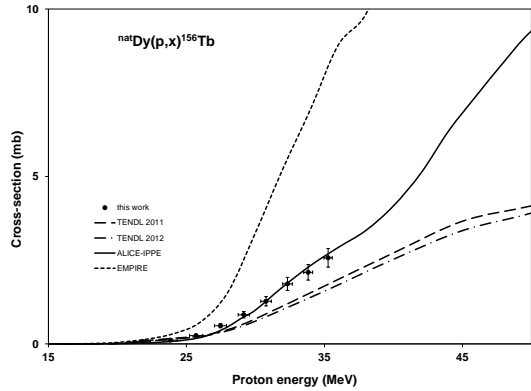


Figure 10: Experimental and theoretical cross-sections for the formation of ^{156}Tb by the proton bombardment of dysprosium

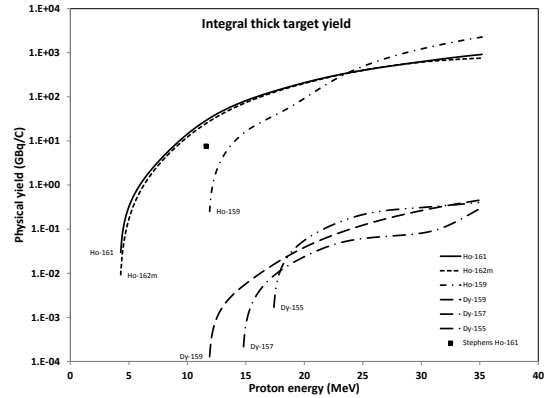


Figure 12: Integral thick target yields for the formation of ^{162m}Ho , ^{161}Ho , ^{159}Ho , ^{159}Dy , ^{157}Dy , ^{155}Dy in proton induced nuclear reaction on ^{nat}Dy as a function of the energy

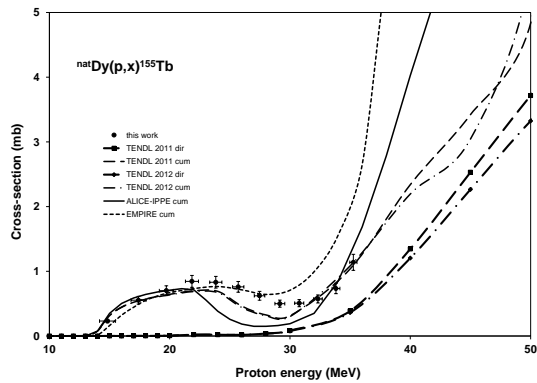


Figure 11: Experimental and theoretical cross-sections for the formation of ^{155}Tb by the proton bombardment of dysprosium

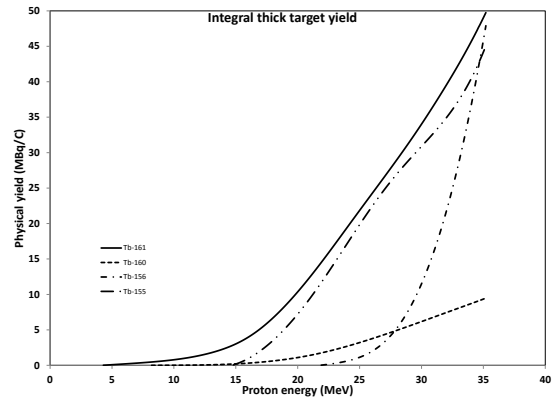


Figure 13: Integral thick target yields for the formation of ^{161}Tb , ^{160}Tb , ^{156}Tb , ^{155}Tb in proton induced nuclear reaction on ^{nat}Dy as a function of the energy

Table 2: Decay characteristics of the investigated reaction products and Q-values of reactions for their productions

Nuclide	Half-life	E_{γ} (keV)	I_{γ} (%)	Contributing reaction	Q-value (keV)
^{162m}Ho IT: 62 % ϵ : 38 %	67.0 min	57.74	4.4	$^{162}\text{Dy}(p,n)$ $^{163}\text{Dy}(p,2n)$ $^{164}\text{Dy}(p,3n)$	-2922.04 -9193.05 -16851.18
^{161}Ho ϵ : 100 %	2.48 h	77.42 103.05 157.26 175.42	1.9 103.05 0.49 0.43	$^{161}\text{Dy}(p,n)$ $^{162}\text{Dy}(p,2n)$ $^{163}\text{Dy}(p,3n)$ $^{164}\text{Dy}(p,4n)$	-1640.64 -9837.63 -16108.65 -23766.77
^{159}Ho ϵ : 99.76 % β^+ : 0.24 %	33.05 m	121.012 131.973 252.963 309.594 838.625	36.2 23.6 13.7 17.2 3.84	$^{160}\text{Dy}(p,2n)$ $^{161}\text{Dy}(p,3n)$ $^{162}\text{Dy}(p,4n)$ $^{163}\text{Dy}(p,5n)$ $^{164}\text{Dy}(p,6n)$	-11195.85 -17650.25 -25847.24 -32118.26 -39776.37
^{159}Dy ϵ : 100 %	144.4 d	58.0	2.27	$^{160}\text{Dy}(p,pn)$ $^{161}\text{Dy}(p,p2n)$ $^{162}\text{Dy}(p,p3n)$ $^{163}\text{Dy}(p,p4n)$ $^{164}\text{Dy}(p,p5n)$ ^{159}Ho decay	-8575.9 -15030.29 -23227.29 -29498.3 -37156.42
^{157}Dy ϵ : 100 %	8.14 h	182.424 326.336	1.33 93	$^{158}\text{Dy}(p,pn)$ $^{160}\text{Dy}(p,p3n)$ $^{161}\text{Dy}(p,p4n)$ $^{162}\text{Dy}(p,p5n)$ $^{163}\text{Dy}(p,p6n)$ $^{164}\text{Dy}(p,p7n)$ ^{157}Ho decay	-9055.54 -24464.14 -30918.53 -39115.52 -45386.54 -53044.66
^{155}Dy ϵ : 98.62 % β^+ : 1.38 %	9.9 h	184.564 226.918	3.37 68.4	$^{158}\text{Dy}(p,p3n)$ $^{160}\text{Dy}(p,p5n)$ $^{161}\text{Dy}(p,p6n)$ $^{162}\text{Dy}(p,p7n)$ $^{163}\text{Dy}(p,p8n)$ $^{164}\text{Dy}(p,p9n)$ ^{155}Ho decay	-25466.2 -40874.7 -47329.1 -55526.1 -61797.1 -69455.3
^{161}Tb β^- : 100 %	6.89 d	74.56669 87.941 103.065 106.113 292.401	10.2 0.183 0.101 0.078 0.058	$^{162}\text{Dy}(p,2p)$ $^{163}\text{Dy}(p,2pn)$ $^{164}\text{Dy}(p,2p2n)$	-8007.59 -14278.6 -21936.72
^{160}Tb β^- : 100 %	72.3 d	86.7877 298.5783 879.378 966.166 1177.954	13.2 26.1 30.1 25.1 14.9	$^{161}\text{Dy}(p,2p)$ $^{162}\text{Dy}(p,2pn)$ $^{163}\text{Dy}(p,2p2n)$ $^{164}\text{Dy}(p,2p3n)$	-7507.17 -15704.16 -21975.17 -29633.29
^{156}Tb ϵ : 100 %	5.35 d	88.97 199.19 262.54 296.49 356.38 422.34 534.29 1065.11 1154.07 1222.44	18 41 5.8 4.5 13.6 8.0 67 10.8 10.4 31	$^{158}\text{Dy}(p,2pn)$ $^{160}\text{Dy}(p,2p3n)$ $^{161}\text{Dy}(p,2p4n)$ $^{162}\text{Dy}(p,2p5n)$ $^{163}\text{Dy}(p,2p6n)$ $^{164}\text{Dy}(p,2p7n)$	-15674.87 -31083.47 -37537.86 -45734.85 -52005.87 -59663.98
^{155}Tb ϵ : 100 %	5.32 d	86.55 105.318 148.64 161.29 163.28 180.08 262.27	32.0 25.1 2.65 2.76 4.44 7.5 5.3	$^{158}\text{Dy}(p,2p2n)$ $^{160}\text{Dy}(p,2p4n)$ $^{161}\text{Dy}(p,2p5n)$ $^{162}\text{Dy}(p,2p6n)$ $^{163}\text{Dy}(p,2p7n)$ $^{164}\text{Dy}(p,2p8n)$ ^{155}Dy decay	-22589.3 -37997.9 -44452.3 -52649.3 -58920.3 -66578.4

Table 3: Experimental cross-sections of $^{nat}\text{Dy}(p,xn)^{162m}\text{Ho}$, ^{161}Ho , ^{159}Ho , ^{159}Dy , ^{157}Dy , ^{155}Dy reactions

E \pm Δ E (MeV)		Cross-section(σ) \pm $\Delta\sigma$ (mb)											
		^{162m}Ho		^{161}Ho		^{159}Ho		^{159}Dy		^{157}Dy		^{155}Dy	
35.3	0.3	34.7	5.7	253.5	34.8	210.0	25.9	270.7	29.4	1.66	0.18	0.36	0.09
33.8	0.3	46.9	5.9	246.2	35.6	241.4	36.1	259.3	28.2	1.01	0.11	0.35	0.07
32.3	0.4	55.6	7.3	293.4	39.0	209.6	25.2	251.4	27.4	0.48	0.06	0.24	0.09
30.8	0.4	82.6	10.2	285.5	38.1	216.0	28.6	264.5	28.8	0.20	0.04	0.28	0.05
29.2	0.4	103.4	11.5	265.0	35.2	176.8	21.1	222.8	24.3	0.08	0.03	0.21	0.06
27.5	0.4	113.6	14.6	214.8	33.2	203.5	38.4	219.4	23.9	0.06	0.03	0.21	0.19
25.7	0.5	114.6	13.1	239.8	32.2	153.3	17.9	191.6	20.9	0.07	0.03	0.52	0.09
23.8	0.5	118.6	13.4	239.2	34.1	137.8	15.8	174.5	19.1	0.13	0.04	0.74	0.08
21.9	0.5	111.1	12.3	248.9	28.1	98.9	11.2	123.8	13.6	0.19	0.03	0.62	0.10
19.7	0.6	93.0	10.4	226.1	25.5	47.1	5.5	132.2	14.4	0.15	0.03	0.53	0.08
17.4	0.6	80.8	9.0	178.8	20.6	18.7	2.5	62.7	6.8	0.11	0.03	0.42	0.08
14.8	0.7	73.0	8.0	156.1	21.1	13.3	1.7	27.7	3.0	0.06	0.02		
11.9	0.7	49.0	5.4	122.3	14.1	5.5	0.7	18.2	2.0				
8.2	0.8	15.3	1.7	39.2	5.8								
4.3	0.9	0.8	0.1	5.7	1.7								

Table 4: Experimental cross-sections of $^{nat}\text{Dy}(p,xn)^{161}\text{Tb}$, ^{160}Tb , ^{156}Tb and ^{155}Tb reactions

E \pm Δ E (MeV)		Cross-section(σ) \pm $\Delta\sigma$ (mb)							
		^{161}Tb		^{160}Tb		^{156}Tb		^{155}Tb	
35.3	0.3	1.11	0.12	2.26	0.26	2.57	0.28	1.14	0.12
33.8	0.3	1.00	0.11	1.84	0.21	2.14	0.23	0.73	0.08
32.3	0.4	0.62	0.08	2.18	0.25	1.79	0.19	0.57	0.06
30.8	0.4	0.96	0.11	2.40	0.27	1.27	0.14	0.51	0.06
29.2	0.4	0.86	0.10	2.22	0.25	0.87	0.10	0.50	0.06
27.5	0.4	0.87	0.10	2.22	0.25	0.54	0.06	0.62	0.07
25.7	0.5	0.88	0.10	2.27	0.26	0.25	0.03	0.76	0.08
23.8	0.5	0.98	0.11	2.01	0.23	0.11	0.01	0.83	0.09
21.9	0.5	0.98	0.11	1.91	0.22	0.07	0.01	0.85	0.09
19.7	0.6	0.90	0.10	1.25	0.14			0.70	0.08
17.4	0.6	0.75	0.08	0.88	0.10			0.55	0.06
14.8	0.7	0.42	0.05	0.49	0.06			0.23	0.03
11.9	0.7	0.23	0.03	0.17	0.02				
8.2	0.8	0.12	0.01	0.01	0.01				
4.3	0.9	0.13	0.01						

References

- Andersen, H. H., Ziegler, J. F., 1977. Hydrogen stopping powers and ranges in all elements. The Stopping and ranges of ions in matter, Volume 3. The Stopping and ranges of ions in matter. Pergamon Press, New York.
- Bonardi, M., 1987. The contribution to nuclear data for biomedical radioisotope production from the milan cyclotron facility.
- Canberra, 2000. http://www.canberra.com/products/radiochemistry_lab/genie-2000-software.asp.
- Dityuk, A. I., Konobeyev, A. Y., Lunev, V. P., Shubin, Y. N., 1998. New version of the advanced computer code alice-ippe. Tech. rep., IAEA.
- Herman, M., Capote, R., Carlson, B. V., Oblozinsky, P., Sin, M., Trkov, A., Wienke, H., Zerkin, V., 2007. Empire: Nuclear reaction model code system for data evaluation. Nuclear Data Sheets 108 (12), 2655–2715.
- Hubner, K. F., Andrews, G. A., Hayes, R. L., Poggenburg, J. K., J., Solomon, A., 1977. The use of rare-earth radionuclides and other bone-seekers in the evaluation of bone lesions in patients with multiple myeloma or solitary plasmacytoma. Radiology 125 (1), 171–6.
- International-Bureau-of-Weights-and-Measures, 1993. Guide to the expression of uncertainty in measurement, 1st Edition. International Organization for Standardization, Geneva, Switzerland.
- Kinsey, R. R., Dunford, C. L., Tuli, J. K., Burrows, T. W., 1997. Nudat 2.6. In: Proceedings of the 9th International Symposium on Capture Gamma Ray Spectroscopy and Related Topics. Springer Hungarica Ltd.
- Koning, A. J., Rochman, D., 2012. Modern nuclear data evaluation with the talys code system. Nuclear Data Sheets 113, 2841.
- Lebowitz, E., Greene, M. W., 1971. The production of ^{157}Dy for medical use. The International journal of applied radiation and isotopes 22 (12), 789–793.
- Muller, C., Zhernosekov, K., Koster, U., Johnston, K., Dorrer, H., Hohn, A., van der Walt, N. T., Turler, A., Schibli, R., 2012. A unique matched quadruplet of terbium radioisotopes for pet and spect and for alpha- and beta- radionuclide therapy: an in vivo proof-of-concept study with a new receptor-targeted folate derivative. Journal of Nuclear Medicine 53 (12), 1951–9.
- Nayak, D., Lahiri, S., 1999. Application of radioisotopes in the field of nuclear medicine - i. lanthanide series elements. Journal of Radioanalytical and Nuclear Chemistry 242 (2), 423–432.
- Neves, M., Kling, A., Oliveira, A., 2005. Radionuclides used for therapy and suggestion for new candidates. Journal of Radioanalytical and Nuclear Chemistry 266 (3), 377–384.
- Pritychenko, B., Sonzogni, A., 2003. Q-value calculator.
- Rosch, F., 2007. Radiolanthanides in endoradiotherapy: an overview. Radiochimica Acta 95 (6), 303–311.
- Stephens, B. J., 2010. ^{161}Ho + iudr: optimized photon activation therapy, phd thesis. Ph.D. thesis.
- Stephens, B. J., Mendenhall, M. H., 2010. Holmium-161 produced using 11.6 mev protons: A practical source of narrow-band x-rays. Applied Radiation and Isotopes 68 (10), 1928–1932.
- Székely, G., 1985. Fgm - a flexible gamma-spectrum analysis program for a small computer. Computer Physics Communications 34 (3), 313–324.
- Takács, S., Tárkányi, F., Hermanne, A., Rebeles, R. A., 2011. Activation cross sections of proton induced nuclear reactions on natural hafnium. Nuclear Instruments & Methods in Physics Research Section B-Beam Interactions with Materials and Atoms 269 (23), 2824–2834.
- Tárkányi, F., Ditrói, F., Hermanne, A., Takács, S., Ignatyuk, A. V., 2013a. Investigation of production routes for the ^{161}Ho auger-electron emitting radiolanthanide, a candidate for therapy. Journal of Radioanalytical and Nuclear Chemistry in print.
- Tárkányi, F., Ditrói, F., Takács, S., Király, B., Hermanne, A., Sonck, M., Baba, M., Ignatyuk, A. V., 2012. Investigation of activation cross-sections of deuteron in-

- duced nuclear reactions on natmo up to 50 mev. Nuclear Instruments & Methods in Physics Research Section B-Beam Interactions with Materials and Atoms 274, 1–25.
- Tárkányi, F., Szelecsényi, F., Takács, S., 1991. Determination of effective bombarding energies and fluxes using improved stacked-foil technique. Acta Radiologica, Supplementum 376, 72.
- Tárkányi, F., Takács, S., Ditrói, F., Csikai, J., Hermanne, A., Ignatyuk, A. V., 2013b. Activation cross-sections of deuteron induced reactions on natgd up to 50 mev. Applied Radiation and Isotopes submitted.
- Tárkányi, F., Takács, S., Gul, K., Hermanne, A., Mustafa, M. G., Nortier, M., Oblozinsky, P., Qaim, S. M., Scholten, B., Shubin, Y. N., Youxiang, Z., 2001. Beam monitor reactions (chapter 4). charged particle cross-section database for medical radioisotope production: diagnostic radioisotopes and monitor reactions. Tech. rep., IAEA.
- Uusjarvi, H., Bernhardt, P., Rosch, F., Maecke, H. R., Forssell-Aronsson, E., 2006. Electron- and positron-emitting radiolanthanides for therapy: Aspects of dosimetry and production. Journal of Nuclear Medicine 47 (5), 807–814.